Article

Cell Stem Cell

Identification and Successful Negotiation of a Metabolic Checkpoint in Direct Neuronal Reprogramming

Graphical Abstract

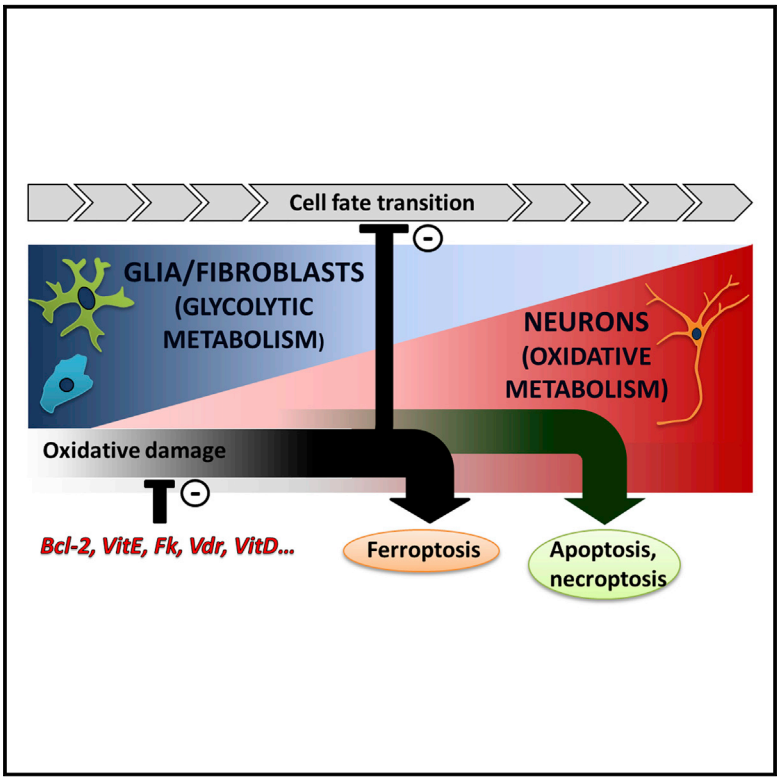

Highlights

- Oxidative stress is a major hurdle in converting different cell types into neurons
- Ferroptosis inhibitors and antioxidants improve direct neuronal reprogramming
- Bcl-2 reduces ROS and promotes direct neuronal reprogramming also in vivo
- Antioxidants potently improve maturation of induced neurons in vitro and in vivo

Authors

Sergio Gascón, Elisa Murenu, Giacomo Masserdotti, ..., Marcus Conrad, Benedikt Berninger, Magdalena Götz

Correspondence

sergio.gascon@med.uni-muenchen.de (S.G.), magdalena.goetz@helmholtz-muenchen.de (M.G.)

In Brief

By imaging cell fate conversion over time, Gascón, Murenu, and colleagues find that high levels of oxidative stress prevent successful direct neuronal reprogramming, instead causing extensive cell death. They identify inhibitors of ferroptosis, antioxidants, and Bcl-2 as key metabolic agents in improving generation of iNs from a range of somatic cells and in vivo after brain injury.

Accession Numbers

GSE70921

Gascón et al., 2016, Cell Stem Cell *18*, 1–14
March 3, 2016
http://dx.doi.org/10.1016/j.stem.2015.12.003

CellPress

Please cite this article in press as: Gascón et al., Identification and Successful Negotiation of a Metabolic Checkpoint in Direct Neuronal Reprogramming, Cell Stem Cell (2016), http://dx.doi.org/10.1016/j.stem.2015.12.003

Cell Stem Cell
Article

Identification and Successful Negotiation of a Metabolic Checkpoint in Direct Neuronal Reprogramming

Sergio Gascón,[1,2,14,*] Elisa Murenu,[1,2,14] Giacomo Masserdotti,[1,2] Felipe Ortega,[1,3,4] Gianluca L. Russo,[1,2] David Petrik,[1,2] Aditi Deshpande,[1,15] Christophe Heinrich,[1,16] Marisa Karow,[1] Stephen P. Robertson,[5] Timm Schroeder,[6,17] Johannes Beckers,[7,8,9] Martin Irmler,[8] Carsten Berndt,[10] José P. Friedmann Angeli,[11] Marcus Conrad,[11] Benedikt Berninger,[1,3,12] and Magdalena Götz[1,2,13,*]

[1]Physiological Genomics, Biomedical Center Ludwig-Maximilians-University Munich, 80336 Munich, Germany
[2]Institute for Stem Cell Research, Helmholtz Center Munich, 85764 Neuherberg, Germany
[3]Institute of Physiological Chemistry, University Medical Center of the Johannes Gutenberg University Mainz, 55128 Mainz, Germany
[4]Biochemistry and Molecular Biology Department, Faculty of Veterinary Medicine, Complutense University, Avenue Puerta de Hierro, 28040 Madrid, Spain
[5]Department of Women's and Children's Health, Dunedin School of Medicine, University of Otago, 9016 Dunedin, New Zealand
[6]Research Unit Stem Cell Dynamics, Helmholtz Center Munich, Neuherberg, 85764 Neuherberg, Germany
[7]German Center for Diabetes Research (DZD), 85764 Neuherberg, Germany
[8]Institute of Experimental Genetics, Helmholtz Center Munich GmbH, 85764 Neuherberg, Germany
[9]Center of Life and Food Sciences Weihenstephan, Technical University Munich, 85354 Freising, Germany
[10]Department of Neurology, Medical Faculty, Heinrich-Heine University Düsseldorf, Merowingerplatz 1a, 40225 Düsseldorf, Germany
[11]Institute of Developmental Genetics, Helmholtz Center Munich, 85764 Neuherberg, Germany
[12]Focus Program Translational Neuroscience, Johannes Gutenberg University Mainz, 55128 Mainz, Germany
[13]Excellence Cluster of Systems Neurology (SYNERGY), 80336 Munich, Germany
[14]Co-first author
[15]Present address: Department of Psychiatry and Institute for Human Genetics, University of California San Francisco, San Francisco, CA 94143, USA
[16]Present address: INSERM, U1216, University Grenoble Alpes, Grenoble Institut des Neurosciences, GIN, F-38000 Grenoble, France
[17]Present address: Department of Biosystems Science and Engineering, ETH Zurich, Mattenstrasse 26, 4058 Basel, Switzerland
*Correspondence: sergio.gascon@med.uni-muenchen.de (S.G.), magdalena.goetz@helmholtz-muenchen.de (M.G.)
http://dx.doi.org/10.1016/j.stem.2015.12.003

SUMMARY

Despite the widespread interest in direct neuronal reprogramming, the mechanisms underpinning fate conversion remain largely unknown. Our study revealed a critical time point after which cells either successfully convert into neurons or succumb to cell death. Co-transduction with Bcl-2 greatly improved negotiation of this critical point by faster neuronal differentiation. Surprisingly, mutants with reduced or no affinity for Bax demonstrated that Bcl-2 exerts this effect by an apoptosis-independent mechanism. Consistent with a caspase-independent role, ferroptosis inhibitors potently increased neuronal reprogramming by inhibiting lipid peroxidation occurring during fate conversion. Genome-wide expression analysis confirmed that treatments promoting neuronal reprogramming elicit an anti-oxidative stress response. Importantly, co-expression of Bcl-2 and anti-oxidative treatments leads to an unprecedented improvement in glial-to-neuron conversion after traumatic brain injury in vivo, underscoring the relevance of these pathways in cellular reprograming irrespective of cell type in vitro and in vivo.

INTRODUCTION

Direct reprogramming of somatic cells has proven to be an extraordinary method to generate cell populations such as neurons that are otherwise difficult to obtain for research purposes (Amamoto and Arlotta, 2014). In addition, replenishing neuronal populations in the injured brain using reprogramming-based therapies is an exciting future prospect (Buffo et al., 2005; Heinrich et al., 2014). However, the cellular and molecular basis underlying direct reprogramming remains poorly understood. Most studies are restricted to the function of neurogenic reprogramming factors (Masserdotti et al., 2015; Ninkovic et al., 2013; Wapinski et al., 2013), while little is known about other aspects, such as metabolic changes or proliferation. As the function of neurogenic factors is context dependent, this also prompts the question to which extent there may be mechanisms common to all cells types converting into neurons. For example, Neurogenin2 (Neurog2) efficiently induces neuronal conversion of mouse postnatal astrocytes in culture (Berninger et al., 2007; Blum et al., 2011; Heinrich et al., 2010) but is rather ineffective in mouse embryonic fibroblasts (MEFs) (Chanda et al., 2014) or adult reactive glial cells in vivo (Grande et al., 2013). While the starting cell type may dictate conversion efficiency by providing transcriptional accessibility of target genes (Wapinski et al., 2013), other cellular processes shown to influence reprogramming into induced pluripotent stem cells (iPSCs) such as cell death (Kawamura et al., 2009), proliferation rate (Halley-Stott et al., 2014; Ruiz

et al., 2011), or metabolic state (Zhang et al., 2012) may also be important in direct neuronal reprogramming. Among them, the metabolic state is particularly relevant for the conversion into neurons, which rely on oxidative metabolism, while astroglia, fibroblasts, and proliferative cells rather utilize anaerobic glycolysis and β-oxidation (McKay et al., 1983; Tsacopoulos and Magistretti, 1996). Moreover, metabolic factors such as reactive oxygen species (ROS) have been implicated in cell fate regulation (Maryanovich and Gross, 2013). Here, we used continuous single-cell live imaging to monitor direct reprogramming of fibroblasts and glia into neurons. We identify stage-specific barriers and metabolic regulators increasing conversion efficiency both in vitro and in vivo.

RESULTS

A Critical Checkpoint Eliciting Cell Death in Neuronal Conversion

To target also postmitotic cells, we transfected astroglial cells isolated from mouse cerebral cortex at postnatal day (P) 5–7 with a dual red fluorescent protein (RFP) and *Ascl*1-encoding vector (Heinrich et al., 2010; Masserdotti et al., 2015) and tracked RFP+ cells starting at 26–29 hr after transfection (Figure 1A). In this model, neuronal conversion is achieved within 7 days and can be monitored by continuous single-cell imaging. Images were taken every 5 min in phase contrast and 5 hr in the fluorescence channel (RFP+; Figure 1B shows stills from such movies; Movie S1). To follow the fate conversion we used three methods: neuronal morphology (Figures 1B–1H and S1A; Movie S1), GFP driven by the Doublecortin promoter (DCX-*GFP*; Figures S2A–S2C; Movie S2), and immunostaining for neuron-specific antigens (Figure 1B, lower panels; Figures S2D and S2E). The first signs of neuronal conversion were visible by weak DCX-*GFP* signals at around 24 hr of live imaging (i.e., about 2 days after transfection, see Figure 1A; Figure S2, blue line) and most cells that became DCX-*GFP*+ did so within the first 2 days of imaging (Figures S2A1, S2B1, and S2C, blue line), i.e., about 3 days after transfection (Figure 1A). Thus, the regulation of key neuronal genes occurs rapidly and is implemented within few days (see also Masserdotti et al., 2015). Within 50 hr of imaging, i.e., about 3 days after transfection, the first Ascl1/RFP+ cells changed from flat astrocyte to neuronal morphology (Figures 1B1 and 1C1). Noteworthy, more than 90% of cells classified with a neuronal morphology were accordingly immuno-reactive for β-III-tubulin and MAP2. The more mature neuronal marker NeuN was present only in 60% of cells with neuronal morphology (Figures S1B and S1C). Among the cells with non-neuronal morphology we found cells in fate transition immunoreactive for both neuronal (β-III-tubulin) and astroglia (GFAP) markers (Figure S1E, upper). Cells with a neuronal morphology were never found to be double positive for GFAP and neuronal markers (Figure S1E, lower), confirming the stringency of these criteria.

By about 150 hr of imaging (7 days post-transfection [DPT]) most RFP+ cells had developed a neuronal morphology (Figures 1B1, 1C1, and 1D, left bars) or DCX-reporter activity (see example in Figures S2A1, S2B1, and S2C, blue line). However, at that time, the number of RFP+ cells had decreased dramatically, with only about 18% of all RFP+ cells observed at the beginning of the time lapse (see Movie S1) surviving to the end (Figures 1B1, 1C1, and 1D, left bars). The peak of cell death occurred between 50- and 100-hr imaging (Figures 1B1, 1C1, and 1D, left bars), when fate conversion manifests by morphological changes (Figures 1B1 and 1C1). Most (94%) transfected cells that did not acquire a neuronal morphology underwent cell death at some point during the observation period (Figures 1D and 1G, left bars), while only 48% of the cells with neuronal morphology died (Figure 1H, left bar). Accordingly, most cells surviving until the end of imaging were reprogrammed into neurons (Figures 1B1, 1C1, and 1D, left bars; Figures S2A1, S2B1, and S2C, blue line). Thus, cell death is a main limiting factor of neuronal reprogramming and peaks at the time of fate conversion. Conversely, proliferation is limited in this paradigm (Figure 1F, left bar), with most astrocytes directly converting into neurons (Figure 1C1).

Bcl-2 Improves Fate Conversion and Survival

To improve survival during reprogramming, we first examined the effect of the anti-apoptotic protein Bcl-2. Indeed, co-expression of *Bcl-2* with *Ascl1*/*RFP* in astrocytes not only increased the total number of surviving cells, but also the number of induced neurons (iNs), based on morphological analysis (Figures 1B–1D), DCX-reporter activity (Figures S2A–S2C), and immunostaining for β-III-tubulin and MAP2 at 5 DPT (Figures S2D and S2E). Furthermore, continuous single cell imaging revealed a faster conversion of *Ascl1*/*Bcl-2* co-transfected astrocytes, with a significant increase in the proportion of cells with neuronal morphology in the initial phases (8-fold at 50 hr of tracking time; Figures 1C–1E; Movie S1) and faster acquisition of DCX-reporter (Figures S2A–S2C; Movie S2) but no effect on cell proliferation (Figure 1F). Bcl-2 expression increased the proportion of surviving cells in the whole transfected population (Figures 1B–1D and S2A–S2C), while each class of cells, i.e., those with neuronal and non-neuronal morphology, still died as much as cells not co-expressing Bcl-2 (Figures 1G and 1H). Thus, the main effect of Bcl-2 is to facilitate fate transition from astrocytes to neurons, which then have a lower death rate (Figure 1I).

Continuous live imaging results were further corroborated by immunostaining and electrophysiology. Indeed, neuronal morphology faster acquired by *Bcl-2* co-expression correlated with lower resting membrane potential (RMP = −60 to −40 mV; Figures S2F and S2G) typical for immature neurons (Pedroni et al., 2014), while astrocytes have a RMP of −90 to −80 mV (Anderová et al., 2004) (Figures S2F and S2G). Notably, at 5DPT, when most reprogrammed cells have already acquired DCX-GFP, β-III-tubulin, MAP2, and NeuN expression (Figures S1C and S1D), their electrophysiological properties are still immature, and only 10% of *Ascl1*/*Bcl-2* co-transfected cells exhibited some very immature action potential-like features (Figure S2F3). However, iNs recorded at 15 DPT showed action potentials consistent with fully developed neurons (Figure S2H). Taken together, these results demonstrate that Bcl-2 improves reprogramming by faster fate conversion.

Bcl-2 Promotes the Efficiency of Neuronal Conversion via a Non-canonical Pathway

As the Bcl-2 effect seems not only related to its anti-apoptotic role, we examined the contribution of its canonical function via

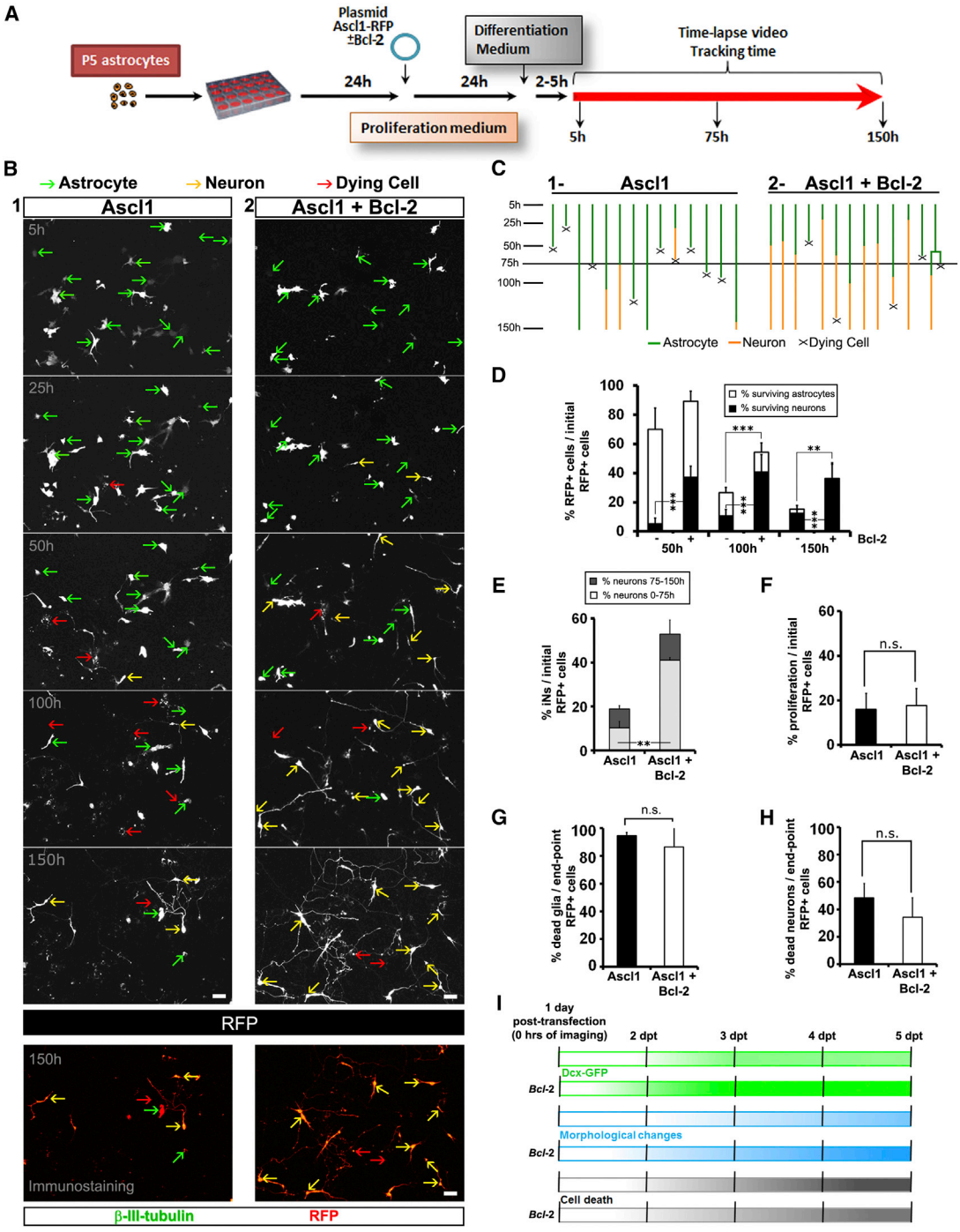

Figure 1. Time-Lapse Analysis of Astrocyte-to-Neuron Reprogramming

(A) Schematic of the experimental protocol used for time-lapse video analysis.

(B) Still images from video-time lapse movies (see Movie S1) showing cells classified as non-neuronal/astroglial (green arrows), neuronal (yellow arrows), and dying (red arrows) at the time in vitro indicated transfected with the constructs indicated.

(C) Progeny-trees of single cells tracked from example in B showing astrocytes (green lines), dead cells (depicted with "x") and neurons (yellow lines).

(D–H) Histograms depicting cell survival and neuronal conversion from movies (n = 5 for control; 339 cells tracked; n = 4 with Bcl-2, 237 cells tracked) based on morphological classification, as detailed and verified by immunostaining in Figures S1A–S1D. The percentage of neurons is normalized to the initial number of transfected cells in (D) and (E).

(I) Schematic summary of reprogramming and cell death as indicated by gradients of the respective color.

Error bars indicate ± SD. $^{**}p < 0.01$, $^{***}p < 0.001$, $p \geq 0.05$, no statistically significant difference (n.s.); ANOVA Tukey's post hoc test in (D); t test in (E)–(G) and (H). Scale bars represent 40 μm. See also Figure S1 and Movies S1 and S2.

the interaction with the pro-apoptotic Bax/Bak. Bcl-2 inhibits apoptosis by sequestering Bax/Bak when phosphorylated at serine 69/70 (Deng et al., 2006) (Figure 2A). The replacement of both Ser69/70 by glutamic acid (EE-*Bcl-2*) mimics the constitutively phosphorylated form of Bcl-2 that sequesters Bax (Figure 2A), while substitution of Ser70 by alanine (A(70)-*Bcl-2*; Figure 2A) mimics the un-phosphorylated form of Bcl-2, reducing the binding to Bax (Deng et al., 2006). Likewise, A(145)-Bcl-2 is unable to bind Bax due to a Glycine145/alanine substitution (Figure 2A; Yin et al., 1994).

Co-expression of EE-*Bcl-2* increased survival of cells transfected with *Ascl1* (Figure 2B), but did not alter the proportion of iNs (blue bars in Figure 2C). As expected, A(145)-Bcl-2 had no significant effect in promoting cell survival during reprogramming (Figure 2B), but surprisingly still increased the proportion of *Ascl1*-transfected cells that turned into neurons (blue bars in Figure 2C). Co-transduction with A(70)-*Bcl-2* still retained some effect on cell survival (comparable to WT-*Bcl-2*; Figure 2B) and was most efficient in neuronal conversion, due to the added effect of rescuing non-converted cells from death and allowing them to convert more efficiently (Figure 2C, gray and blue bars, respectively). Moreover, we also observed increased length and complexity of the neuronal processes in cultures co-transfected with WT-*Bcl-2*, A(70)-*Bcl-2*, or A(145)-*Bcl-2*, but not with EE-*Bcl-2* (Figure 2D), further supporting an additional non-apoptotic role of Bcl-2 in neuronal reprogramming.

Importantly, Bcl-2 also enhanced conversion efficiency obtained from astrocytes transduced with *Neurog2* (Figure 2E), which induced mature glutamatergic neurons (vGlut1+ cells, Figure 2F). Both WT-*Bcl-2* and, to a greater extent, A(70)-*Bcl-2* potently enhanced reprogramming of MEFs in combination with a single neurogenic fate determinant (*Ascl1*, Figures 2H, 2I, S3A, and S3C; *Neurog2*, Figures S3B, S3E, and S3F), giving rise to functional neurons able to fire action potentials (Figure S3D). Notably, Bcl-XL, a member of the Bcl-2 family, had a similar effect on reprogramming as WT-Bcl-2 (data not shown). However, in the absence of a neurogenic factor neither A(70)-*Bcl-2* nor any other *Bcl-2* construct nor *Bcl-XL* alone were able to induce neuronal conversion (Figures 2G and S3C; data not shown). We thus conclude that Bcl-2-related proteins act as a potent facilitators of direct neuronal reprogramming for different transcription factors in different cell types and do so most potently in the A(70)-Bcl-2 mutant form.

Mode of Cell Death in Neuronal Reprogramming

As EE-Bcl-2, the mutant that exhibits an improved anti-apoptotic function, increases cell survival but does not improve the proportion of iNs, we tested how different modes of cell death affect neuron numbers. The pan-caspase/apoptosis inhibitor Z-VAD-FMK (ZVAD, 20 μM) was added once at day 2 to *Ascl1*-transfected astrocytes, resulting in a significant increase in surviving cells (Figure 3A) without affecting the proportion of iNs neither among the initially transfected cells (Figure 3B, gray bars) nor at the end point (Figure 3B, blue bars). Thus, like EE-Bcl-2, blocking caspase activation does not improve neuronal conversion. We then tested the effects of RIP-K dependent necroptosis and the oxidative stress-dependent ferroptosis (Dixon et al., 2012) by using their respective inhibitors Necrostatin-1 (Degterev et al., 2005) and Liproxstatin-1 (Friedmann Angeli et al., 2014). While Necrostatin-1 had similar effects to ZVAD in rescuing some cells from death (Figure 3A), but no effects on iNs (Figure 3B), Liproxstatin-1 had a potent effect on conversion efficiency (Figure 3B). Thus, while apoptosis and necroptosis inhibitors protect cells from death, only the ferroptosis inhibitor liproxstatin-1 promotes both survival and neuronal conversion.

Increased Lipid Peroxidation during Neuronal Reprogramming

Given the positive effects of Liproxstatin-1 treatment on reprogramming efficiency, we next examined lipid peroxidation (Lip-Ox) as a hallmark of ferroptosis (Dixon et al., 2012) by using two different reporters: Click-iT lipid peroxidation kit based on linoleamide alkyne (LAA) reagent (Life technologies) and C11-Bodipy (Drummen et al., 2002). Astrocyte cultures treated with cumene hydroperoxide as a positive control for Lip-Ox had increased signal from the LAA-based reporter in almost all cells (Figure 3C, upper row). Without any additional treatment, 60% of *Ascl1*-transfected cells exhibited the signal for Lip-Ox at 3 DPT, in contrast to 25% of cells transfected with the control plasmid (Figures 3C and 3D), suggesting that Lip-Ox occurs primarily during neuronal reprogramming. Similar results were obtained with C11-Bodipy, which integrates into phospholipid-containing membranes and shifts from red to green fluorescence upon oxidation (Drummen et al., 2002). We also tested α-Tocopherol (αToc, one of the forms of vitamin E, 20μM), known to protect against Lip-Ox (Buettner, 1993), and found that it strongly reduces Lip-Ox LAA-signal in astrocytes undergoing neuronal conversion (Figures 3C and 3D).

Given the non-canonical effect of Bcl-2 on neuronal reprogramming, we examined its effect on Lip-Ox. Indeed, all forms of Bcl-2 significantly reduced Lip-Ox, with EE-Bcl-2 being the weakest and A(70)-Bcl-2 the strongest (Figure 3D). This result was observed with both reporters (Figures 3D and 3E), demonstrating a novel role of Bcl-2 in protecting from Lip-Ox most potently in the A(70)-Bcl2 mutant form. Consequently, we hypothesized that any condition that reduces Lip-Ox should be beneficial for direct neuronal reprogramming. Indeed, αToc treatment, almost doubled the proportion of *Ascl1*/*RFP* reprogrammed neurons obtained from astrocytes at 5DPT (Figures 4A–4C) and improved conversion efficiency of cells co-treated with ZVAD or co-expressing Ascl1/EE-Bcl-2 (Figures 4A and 4B). Thus, the anti-oxidant vitamin E improves direct neuronal reprogramming.

Forskolin Promotes the Efficiency of Neuronal Conversion and Reduces Lipid Peroxidation

We next tested whether other molecules known to improve reprogramming such as forskolin (Fk; Liu et al., 2013a) may also alleviate Lip-Ox. First, we verified its positive effects on reprogramming in astrocytes aiming to determine whether it would act similarly from what we had observed with Bcl-2. Both in continuous live imaging (Figures S4A–S4D) and after immunostaining at 5DPT (Figures 4D and 4E) we observed more cells surviving and efficiently converting after addition of 20 μM Fk to *Ascl1*-transfected astrocyte cultures. As for Bcl-2, we also observed a faster conversion (Figures S4A–S4D) without any

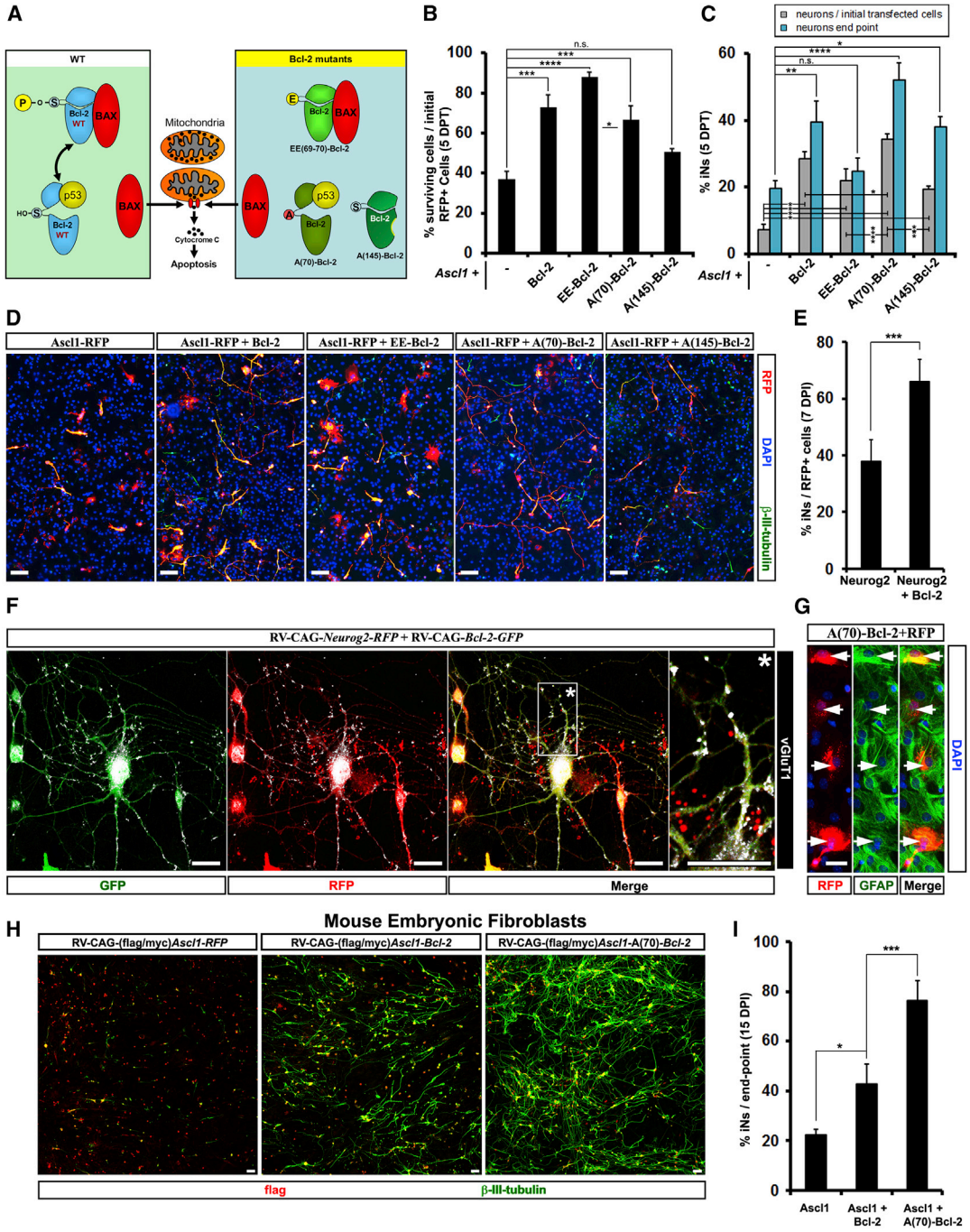

Figure 2. Non-canonical, BAX-Independent Effect of Bcl-2 on Neuronal Reprogramming

(A) Cartoon depicting previously described interactions of Bcl-2 and its mutant forms with several molecular partners as described in the text.

(B–D) Histograms (with corresponding micrographs showing immunostaining for β-III-tubulin, in D) depicting the survival and fate conversion rate at 5DPT (for details, see Supplemental Information) in astroglial cultures transfected with the constructs indicated (n = 3; cells = 900–2,500 for each condition).

(E and I) Histograms showing the proportion of β-III-tubulin+ neurons at 7 days post infection (DPI) of astrocytes with a viral vector containing Neurog2 alone or with Bcl-2 (E, n = 3; cells = 1,500–2,000 for each condition) or 15 DPI of MEFs with the vector indicated (I, n = 3; cells = 340–700 for each condition).

(F) Confocal micrographs showing that iNs from E are immunoreactive for vGluT1 at 15 DPI.

(G) Arrows indicate astrocytes co-transfected with Bcl-2 and RFP (Red cells) being immuno-positive for GFAP (green) and retaining astroglial morphology at 7 DPT.

(H) Micrographs of fibroblast conversion into neurons (β-III-tubulin+ cells; green) at 15 DPI upon transduction with retroviral vectors of the constructs indicated. Error bars indicate ± SD. *p < 0.05, **p < 0.01, ***p < 0.001; ANOVA with Tukey's post hoc test in (B), (C), and (I); t test in (E). Scale bars represent 50 μm in (D) and (H) and 10 μm in (F). See also Figure S2.

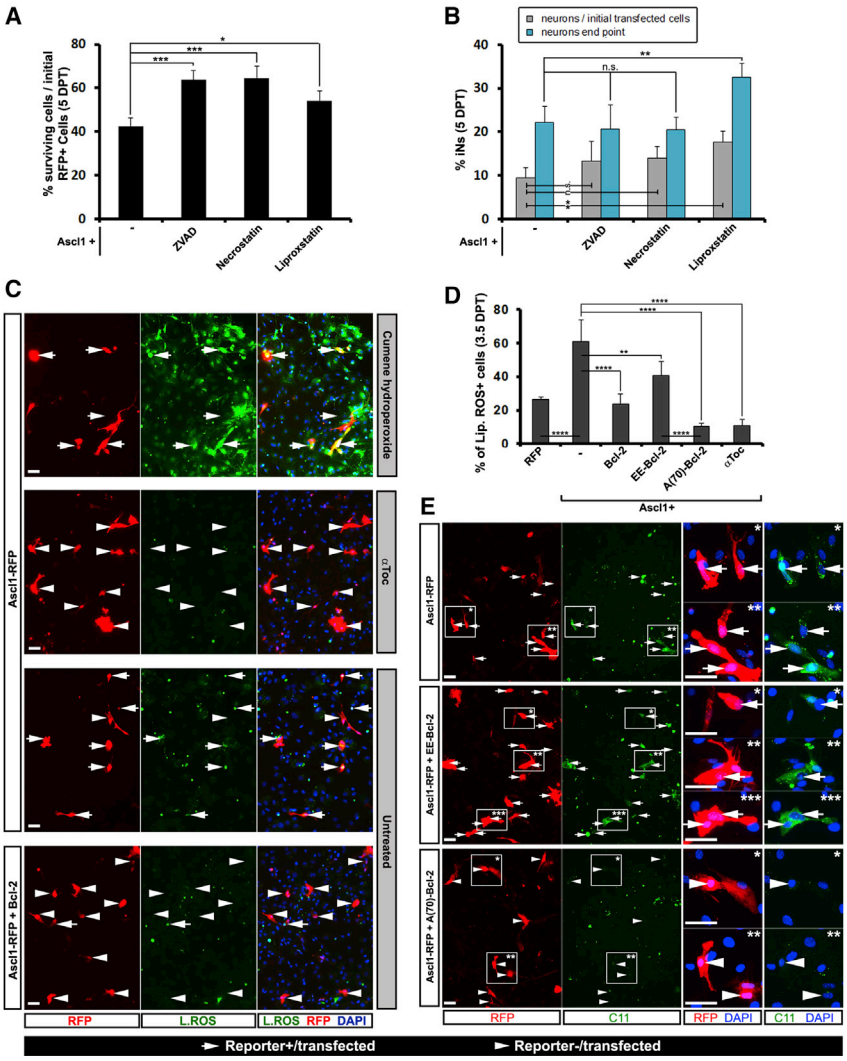

Figure 3. Ferroptosis and Lipid Peroxidation Are Key Limiting Factors during Neuronal Reprogramming

(A, B, and D) Histograms showing the percentage of survival and iNs (A and B) or Lipid ROS+ cells (D, n = 3, for RFP, Bcl-2, A(70)-Bcl-2, αToc; n = 4 for EE-Bcl-2 and Ascl1; cells = 80–500 each condition) in astroglial cultures treated as indicated on the x axis. Treatment with ZVAD (20 μM), Necrostatin (10 μM), or Liproxstatin-1 (200 nM) was performed at 1 DPT (n = 4, A and B; cells = 1,500–2,000).

(C and E) Confocal micrographs of Lip-Ox (Life Technologies, green reporter) staining (C, treatment with cumene hydroperoxide 100 μM; positive control for Lip-Ox, or αToc 10 μM; negative control for Lip-Ox, at 1 DPT) or C11-Bodipy (E) in astrocytes transfected as indicated at 3.5 DPT. Arrows indicate transfected cells (red) with increased levels of Lip-Ox (green); arrowheads show transfected cells without green signal.

Error bars indicate ± SD. *$p < 0.05$, **$p < 0.01$, ***$p < 0.001$; ANOVA with Tukey's post hoc test in (B) and (D); ANOVA with Dunnett's post hoc test in (A). Scale bars represent 40 μm. See also Figure S3.

effect on proliferation (Figure S4E). This effect is both transcription factor and cell type independent, as Fk also improved reprogramming efficiency of MEFs and pericytes (Figure S5) mediated by different transcription factors (i.e., Ascl1, Neurog2, Sox2) but did not induce neuronal conversion in absence of any neurogenic fate determinant (Figures S4F and S5C).

As expected, the proportion of Lip-Ox reporter-positive cells among *Ascl1*-transduced astrocytes was significantly reduced from about 60% to below 20% by Fk treatment (Figures 4F and 4G). Likewise, CellRox Green reagent (Molecular Probes; Figure 4H) showed high levels of nuclear green fluorescence in *Ascl1*-transduced astrocytes at 3DPT, when many cells succumb to cell death, which was reduced after Fk treatment (Figure 4H). As further proof of oxidation-dependent processes occurring during reprogramming, we monitored the oxidation of peroxiredoxin-2, a protein involved in oxidative stress detoxification (Prx2; Godoy et al., 2011), by western blot. Prx2 was predominantly detected in its dimeric (oxidized) form in astrocytes and MEFs 3 days after transduction with *Ascl1*, and dimerization was reduced by Fk treatment (Figure 4I). Thus, reducing oxidative stress during reprogramming facilitates neuronal conversion.

Genome-wide Expression Analysis Reveals Anti-oxidative Stress Response in Improved Neuronal Reprogramming

To identify candidate genes regulated by non-canonical Bcl-2 function and by Fk treatment that may promote neuronal conversion, we collected mRNA from different batches of MEF cultures. These were transduced with *Ascl1/RFP*- or *RFP*-encoding vectors and treated or untreated with Fk for 24 hr (1DPT) or co-transduced with A(70)-*Bcl-2-GFP* (Figure 5A). Upon Fk treatment, 507 probe sets were significantly regulated ($p < 0.01$, fold change $\geq 1.5\times$, see Table S1; for genes regulated after A(70)-*Bcl-2* co-transduction, see Table S2). Heat maps show the 60 strongest upregulated genes upon Fk treatment of *Ascl1*-transduced cells (Figure 5B, left) and the subset of transcriptional regulators (right). The reliability of the transcriptome analysis was confirmed by quantitative real-time PCR analysis (Figure 5C). As expected from the known role of Fk, we found increased expression of genes involved in the cAMP signaling pathway (Table S3) and many targets of Creb, including those regulating neurite outgrowth and cAMP-signaling mediators (Tables S1 and S3), as well as genes promoting neuronal differentiation (e.g., Prox1, Eya2, Sox11; Figure 5B). In addition, we found enrichment of several signaling pathways (e.g., IL-10 and IL-1; Wnt, Bmp) and nuclear receptors (Figure 5B; Table S3). Interestingly, some of these genes, including Nrf-2 effectors and JAK/STAT (Tables S1 and S3), are known to regulate metabolism and the oxidative stress response (Nguyen et al., 2009; Park et al., 2012). Gene Ontology (GO) term analysis further supported anti-oxidative

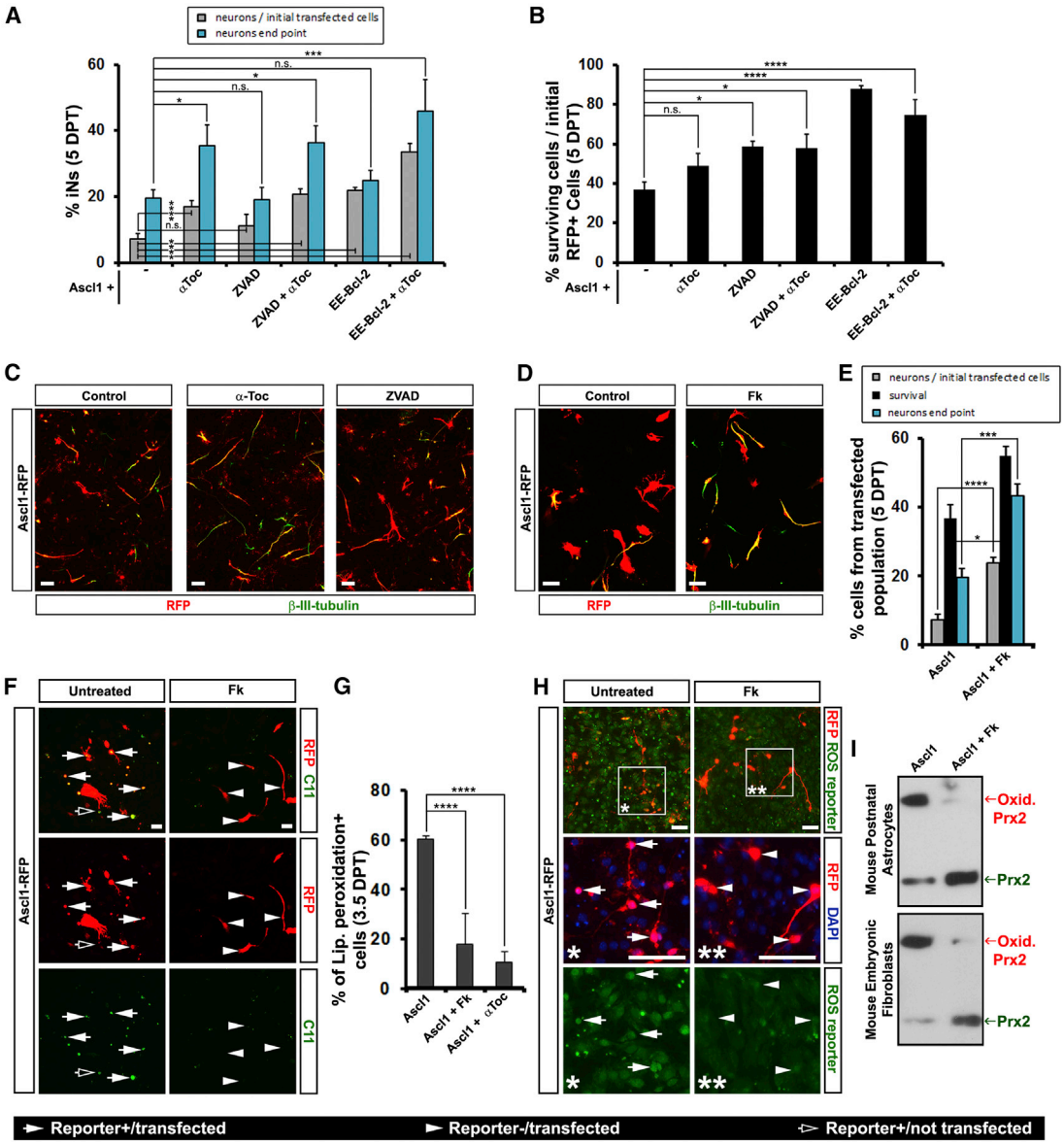

Figure 4. Increased Reprogramming Mediated by a Reduction of Lipid Peroxidation Levels Is Reproduced by Treatment with Forskolin

(A–C) Histograms show iNs (β-III-tubulin+; green in micrographs in C) and survival rate at 5 DPT from astroglial cells transfected and treated as detailed in Figure 3 (n = 3; cells = 1,500–2,000).

(D and E) Micrographs (D) and histogram (E, n = 3; cells = 110–200) of survival rate/neuronal conversion of astroglia transfected with *Ascl1/RFP* (red cells) and cultured 5 days in absence/presence of 10 μM Fk. Neuronal conversion was monitored by β-III-tubulin (green).

(F and H) Micrographs showing examples of the C11-Bodipy reporter (F) or CellROX reporter (green in H) in astrocyte cultures transfected and treated as indicated at 3.5 DPT. Arrows depict transfected cells (red) with increased levels of ROS (green); empty arrows depict untransfected cells; arrowheads show transfected cells with low ROS signal.

(G) Quantification of cells depicted in (F). The result with αToc treatment has been included to compare with the effect of Fk (n = 3 for Ascl1 + αToc; n = 4 for Ascl1 and Ascl1+Fk; cells = 80–250).

(I) Immunoblots showing that 24-hr treatment with Fk reduces the levels of oxidized Prx2 (dimer, upper band) in both astroglial (upper) and MEF (lower) cultures infected with *Ascl1/RFP*-encoding vectors.

Error bars indicate ± SD. *p < 0.05, **p < 0.01, ***p < 0.001; ANOVA with Dunnett's post hoc test in (A), (B), and (E); ANOVA with Tukey's post hoc test in (G). Scale bars represent 40 μm in (C) and (D), 20 μm in (F), and 80 μm in (H). See also Figure S4 and Movie S3.

pathways activated by Fk, with Nrf2-mediated pathway at the top (Table S3). Indeed, we confirmed increased Nrf2-responsive luciferase activity 15 hr after Fk addition (Figure 5D). Interestingly, Nrf2-mediated pathway was found activated by both Fk treatment and A(70)-Bcl-2 co-expression (Table S4). These data support the notion of excessive oxidation occurring during reprogramming and Fk as well as A(70)-Bcl-2 alleviating this.

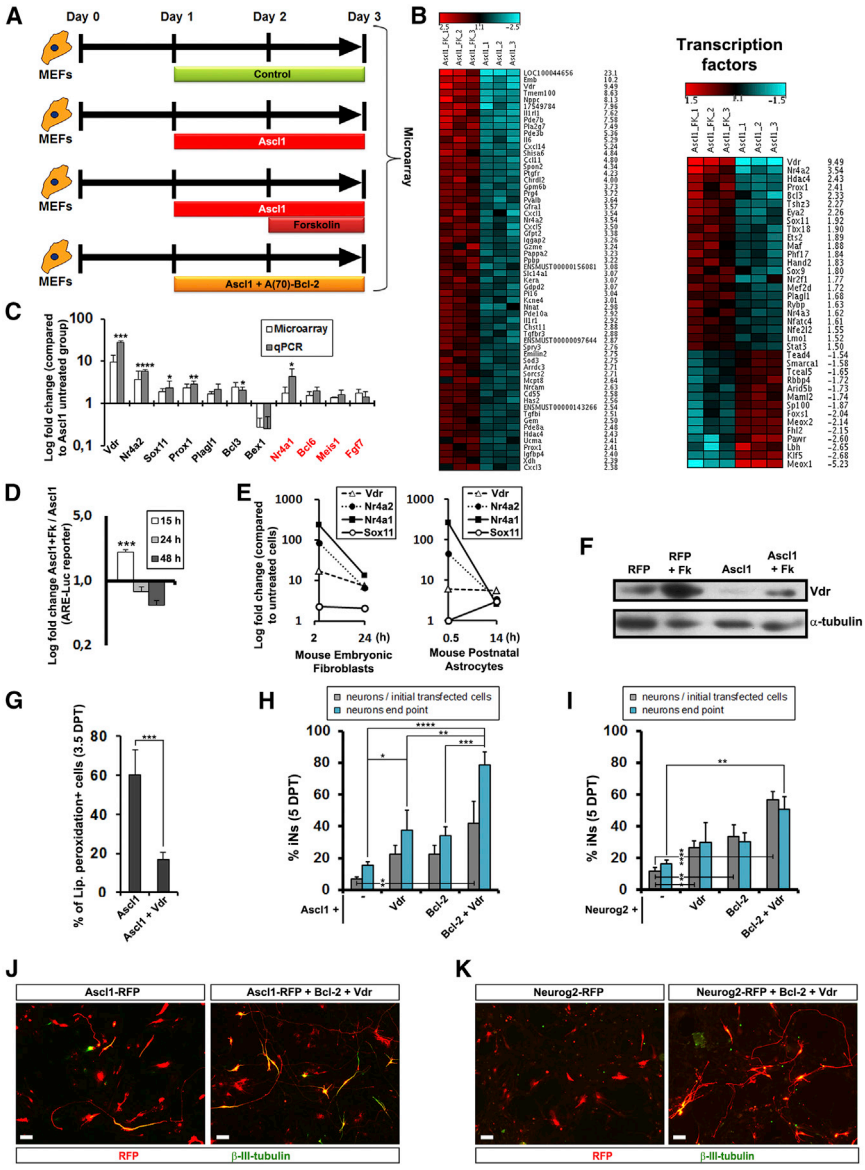

Figure 5. Transcriptome and Functional Analysis of Genes Activated by Fk and Bcl-2

(A) Schematic drawing of the experimental protocol.

(B) Heatmaps of linear fold changes with the top 60 upregulated genes (left) or transcriptional regulators (right) in microarrays of Ascl1+Fk versus Ascl1 only transduced MEFs; $p < 0.01$, fold-change ≥ 1.5.

(C) Histogram showing qRT-PCR for genes predicted to be regulated by the microarray analysis (ratio paired t test, $p < 0.01$; FC ≥ 1.5). Genes with lower significance were also validated ($p < 0.07$; shown in red).

(D) Bars represent fold change of luciferase levels from a Nrf2-responsive construct co-transfected with Ascl1 in astroglial cultures induced by Fk (15, 24, and 48 hr) compared with untreated cells.

(E) qRT-PCR analysis of mRNA levels from four representative targets induced by Fk in MEFs and astrocytes.

(F) Western blot depicting levels of Vdr protein after 24-hr treatment with Fk in astroglia cultures infected with *RFP*- or *Ascl1/RFP*-encoding retroviral vectors.

(G) Percentage of astrocytes positive for the lipid reporter based on linoleic acid (Life Technologies) among the *Ascl1*- or *Ascl1+Vdr*-transfected population at 3.5 DPT. n = 3.

(H–K) Histograms and corresponding micrographs (J and K) depicting the neuronal conversion efficiency of astroglial cultures transfected with constructs indicated on x axis at 5 DPT (n = 3; cells = 80–250).

*$p < 0.05$, **$p < 0.01$, ***$p < 0.001$, ****$p < 0.0001$; ratio paired t test in (C); two-way ANOVA with Sidak's post hoc test in (D); t test in (G); ANOVA with Tukey's post hoc test in (G) and (H); ANOVA with Dunnett's comparison test in (I). Scale bars represent 45 μm. See also Figure S5 and Tables S1, S2, S3, and S4.

As vitamin D receptor (Vdr) was already implicated in the anti-oxidative stress response (Bao et al., 2008; Dong et al., 2012), we validated its upregulation at mRNA level in MEFs and astrocytes (Figure 5E; see also confirmation of other nuclear receptors) and protein level in astrocytes (Figure 5F). We then tested its effect on Lip-Ox in astrocytes and found that co-expression of *Vdr* reduced the percentage of cells positive for LAA-based reporter to less than one-third in *Ascl1*-transfected astrocytes at 3.5 DPT (Figure 5G). Accordingly, co-transfection with *Vdr* improved neuronal reprogramming by *Ascl1* or *Neurog2* to a similar extent as Fk (data not shown) or *Bcl-2* co-transfection (Figures 5H–5K). Co-transduction of *Bcl-2* and *Vdr* further increased reprogramming (Figures 5H–5K) reaching up to 80% neurons among *Ascl1*-transduced astrocytes (Figures 5H and 5J). Taken together, genome-wide expression analysis confirmed the key role of oxidative stress response in regulating reprogramming, with Vdr as the top transcriptional regulator.

The Role of Bcl-2 and Anti-oxidants in Neuronal Reprogramming In Vivo

We next examined the relevance of the above-identified pathways after brain injury in vivo. Such lesions induce a highly inflammatory environment (Abdul-Muneer et al., 2015) that may impose oxidative stress and other metabolic constrains to the generation and survival of iNs. Indeed, in the intact striatum and cerebral cortex, neuronal reprogramming was more efficient (Guo et al., 2014; Niu et al., 2013; Torper et al., 2013) than after large invasive brain injury (Buffo et al., 2005; Grande et al., 2013; Heinrich et al., 2014). Among the previously tested factors, we chose *Neurog2*, as it instructs glutamatergic neurons in the developing cerebral cortex (Imayoshi and Kageyama, 2014) and from astrocytes in vitro (Berninger et al., 2007; Heinrich et al., 2010; Masserdotti et al., 2015), but exhibits a limited efficiency in neuronal conversion after brain injury in vivo (Grande et al., 2013).

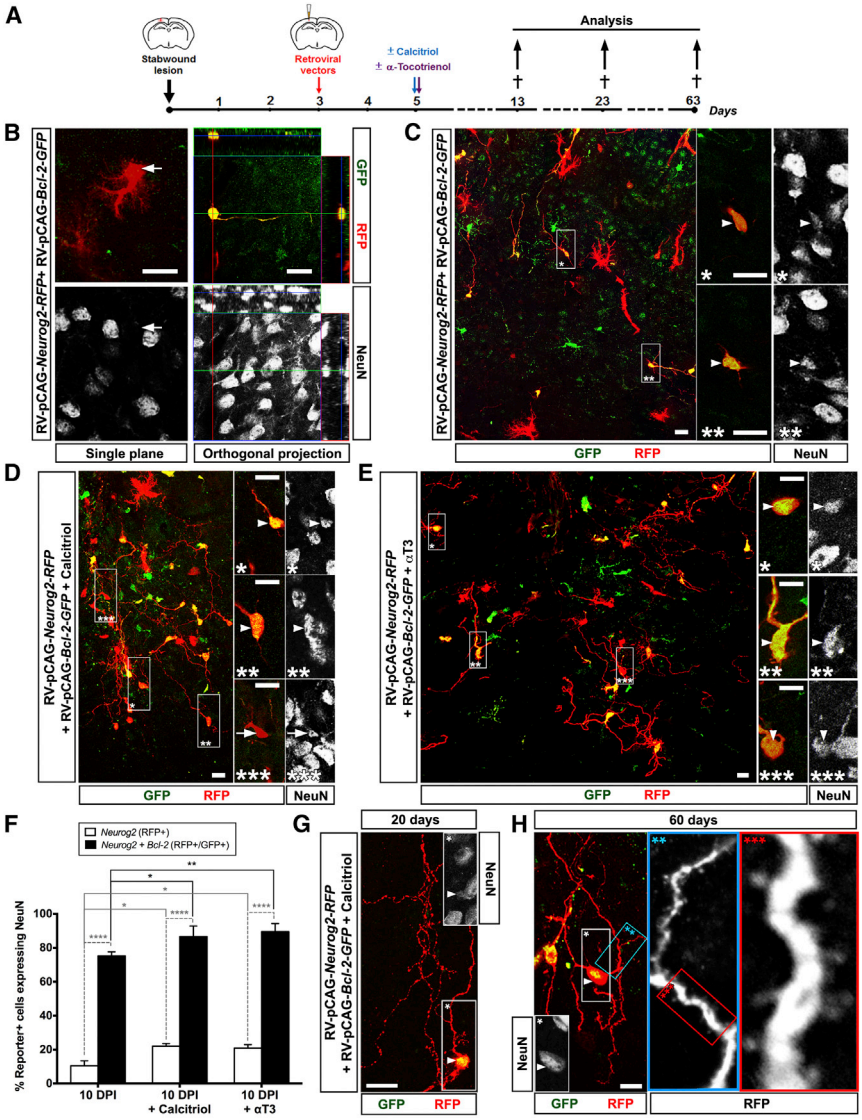

Figure 6. Conversion of Reactive Glia into Neurons Is Improved by *Bcl-2*, Calcitriol, and α-Tocotrienol In Vivo

(A) Scheme of the protocol used for stab-wound injury and subsequent infection with retroviral vectors for *Neurog2*-IRES-*RFP* and *Bcl-2*-IRES-*GFP*, the respective treatments and analysis time points.

(B) High-power micrograph of cells infected by *Neurog2*-IRES-*RFP* alone or with *Bcl-2*-IRES-*GFP* stained for NeuN at 10 DPI, with orthogonal projections of the confocal stack. The RFP+ cell maintains an astroglial morphology and is NeuN-immunonegative (arrows, left), whereas the co-infected cell displays a distinct neuronal-like morphology and NeuN signal (right).

(C–E) Confocal micrographs of the injection site at 10 DPI upon the treatments indicated (C, none; D, Calcitriol; E, αT3) stained for NeuN. Co-infected cells immunopositive for NeuN (arrowheads) are shown at higher magnification in single optical sections (*, **, ***; right).

(F) Histogram with the proportion of induced, NeuN+ neurons among RFP+ and RFP+/GFP+ cells at 10 DPI, without (n = 3) or with treatments (calcitriol, n = 3; αT3, n = 4; 390-575 cells per condition).

(G and H) Micrographs of maximum intensity projections of neuronal examples as indicated. Inserts show single optical section of the NeuN+ nucleus (*; white arrow). The blue and red boxes in H (**, ***) display higher magnifications of a process with spine-like structures.

Error bars indicate ± SD. *$p < 0.05$, **$p < 0.01$, ****$p < 0.0001$; two-way ANOVA with Tukey's post hoc test in (F). Scale bars represent 10 μm, except 20 μm in (B). See also Figure S6.

Retroviral vectors encoding *Neurog2*-IRES-*RFP* alone or in combination with *Bcl-2*-IRES-*GFP* were injected close to the stab-wound injury site 3 days later (Figure 6A), as previously described (Buffo et al., 2005; Heinrich et al., 2014), and immunohistochemistry was performed at 10 days post-injection (DPI). *GFP* or *Bcl-2* single (GFP+) infected cells were NG2+ glia or S100β/GFAP+ astrocytes (Figures 6C and S6C). Similarly, most of the cells transduced with *Neurog-2* (RFP+ only) were glia and only rarely acquired the neuronal marker NeuN (Figures 6B, 6C, and 6F; 2% in only *Neurog2*-infected brains, Figure S6D). Conversely, many co-transduced cells (GFP+/RFP+) exhibited elongated neuronal-like morphology and were immuno reactive for DCX or NeuN (Figures 6C and S6E). Indeed, around 75% of co-transduced cells had turned into NeuN+ neurons with a clear neuronal morphology at 10 DPI (Figure 6F). Taken together, the addition of Bcl-2 not only increased the number of NeuN+ iNs but also accelerated neuronal maturation, as appearance of NeuN typically takes about 14–21 DPI (Grande et al., 2013). Thus, as in vitro, Bcl-2 potently improves reprogramming speed and efficiency in vivo.

We next examined whether activating the Vdr pathway by the ligand calcitriol after *Neurog2/RFP* transduction with/without *Bcl-2/GFP* would elicit a further improvement in reprogramming. Strikingly, a single calcitriol administration at 2 DPI more than doubled the proportion of NeuN+ iNs in *Neurog2*-transduced cells (Figures 6D and 6F; 3.5-fold increase in only *Neurog2*-infected brains, see Figure S6D). Most importantly, calcitriol treatment resulted in almost 90% conversion of all *Neurog2/Bcl-2* co-transduced cells (GFP+/RFP+; Figures 6D and 6F), dramatically increased levels of NeuN (see Figures S6F and S6G) and improved morphology and complexity of iNs, resulting in the formation of long neuronal processes (Figures 6G and S6G). Moreover, long-term analysis of iNs after calcitriol treatment often revealed very elaborate neurites with bouton-like (20 DPI; Figure 6G) and/or spine-like structures (60 DPI; Figure 6H). Taken together, these data demonstrate that calcitriol has a beneficial effect on the reprogramming efficiency but more importantly on the maturation of iNs.

To confirm that the oxidative state directly affects reprogramming in vivo, we administered α-Tocotrienol (αT3; Figure 6A), the vitamin E analog described above. Similarly to calcitriol, αT3 administration improved the conversion efficiency and

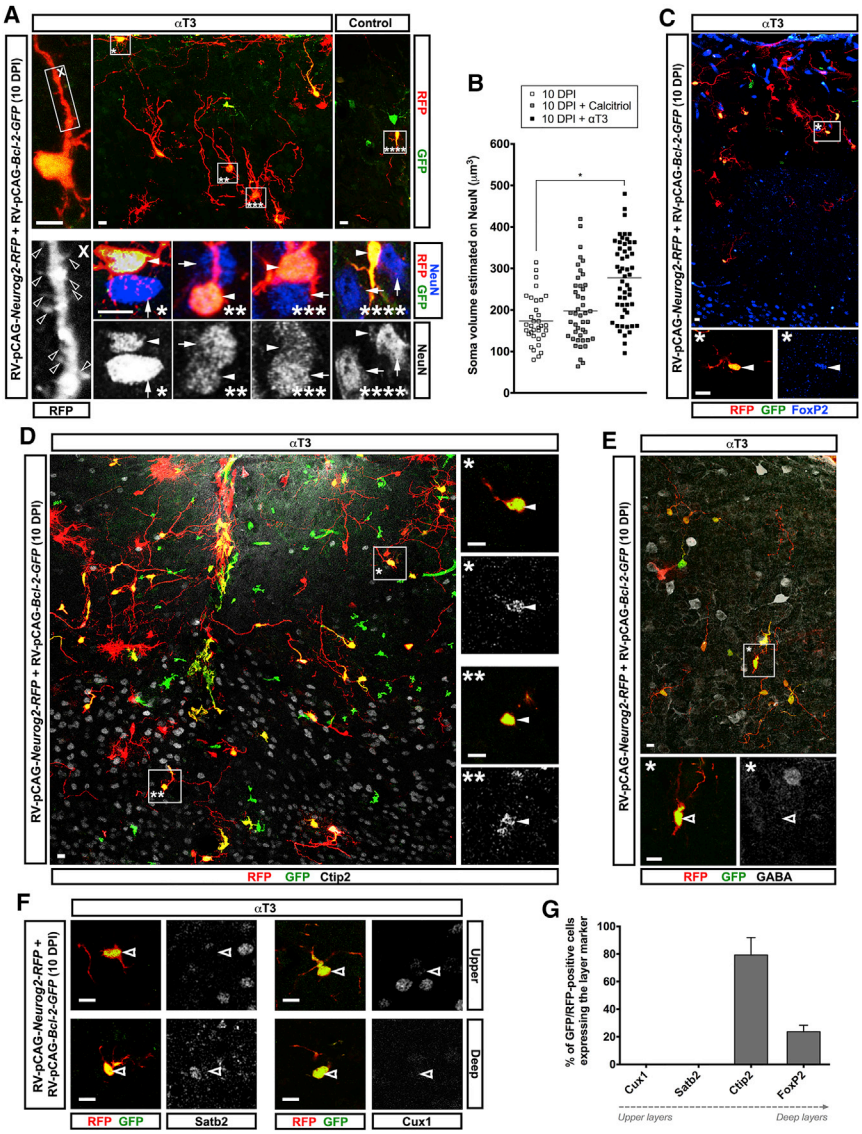

Figure 7. Subtype Identity of iNs after Stab-Wound Injury

(A and B) Confocal micrographs (maximum intensity projection, A) and histogram of soma size (B) of cells at 10 DPI by *Neurog2/RFP* and *Bcl-2/GFP* retroviral vectors after stab-wound injury and αT3 treatment (see Figure 6A) with thick processes and spine-like structures (box X, left). The soma size of these cells (NeuN staining, magnified in boxes *, **, ***; arrowheads) is similar to the size of nearby endogenous neurons (arrows), unlike for mice that did not receive αT3 (right, magnified in ****).

(C–F) Confocal micrographs showing neuronal subtype markers FoxP2 (C), Ctip2 (D), GABA (E), Satb2, and Cux1 (F) at 10 DPI. Filled arrowheads indicate immunopositive, empty arrowheads immunonegative cells in the squared box (*, **). Specific examples of cells located in upper or deep layers are depicted in (F).

(G) Histogram of double infected cells expressing the indicated markers.

Horizontal lines in (B) indicate the mean. n = 4 in A and B (αT3); n = 3 in B (no treatment and calcitriol, 40-60 cells per condition), (C), (D), and (G) for Ctip2 and FoxP2 (80-180 cells per condition); n = 2 in (E), (F), and (G) for Cux1 and Satb2 (40-60 cells per condition). *$p < 0.05$; one-way ANOVA with Tukey's post hoc test in (B). Scale bars represent 10 μm. See also Figure S7.

the levels of NeuN (Figures 6E and 6F). Strikingly, cells co-transduced with *Neurog2/Bcl-2* displayed a very complex neuronal morphology in animals treated with αT3 already at 10 DPI (Figures 6E and 7A) and had a soma size comparable to the endogenous neurons in the same area (Figures 7A and 7B). Notably, iNs also reached this soma size after calcitriol administration, but at a much later time points (60 DPI; see Figures 7A and S6H). Likewise, upon αT3 treatment, iNs exhibited the first spine-like protrusions already at 10 DPI (Figure 7A, left), further corroborating the faster iN differentiation and maturation elicited by this anti-oxidant.

As *Neurog2/Bcl-2* overexpression and αT3 administration resulted in most developed iNs, we used this paradigm to determine their subtype identity. Regardless of the localization of the co-transduced cells, about 80% were immunopositive for Ctip2 (Figures 7D and 7G), a marker for layer V subcortical neurons (Arlotta et al., 2005; Molyneaux et al., 2007). Most of the remainder (20%) was positive for the deep layer marker FoxP2, albeit with lower intensity than endogenous neurons (Figures 7C and 7G; Molyneaux et al., 2007). Consistent with a V pyramidal neuron identity, iNs were negative for the upper layer markers Satb2 (Figures 7F, left, and 7G; Britanova et al., 2008) or Cux1 (Figures 7F, right, and 7G; Molyneaux et al., 2007) and the interneuron transmitter GABA (Figure 7E). Therefore, we confirmed the identity of reprogrammed cells as deep layer glutamatergic pyramidal neurons, consistent with the role of Neurog2 in cortical development (Schuurmans et al., 2004).

DISCUSSION

Here we used continuous live imaging to unravel critical hurdles in direct neuronal reprogramming. Neuronal conversion became detectable around 2–4 days after transduction by live neuronal (DCX-*GFP*) reporters, post-imaging immunostaining (β-III-tubulin, MAP2, NeuN), and morphological analysis (small cell soma and thin processes). At around the same time, most transduced astrocytes succumbed to cell death, while fewer of the successfully converted cells died, suggesting that high levels of Ascl1 may be incompatible with astrocyte survival under these conditions. Importantly, few astrocytes proliferated—neither prior to cell death nor prior to fate conversion. Thus, a major limitation in reprogramming efficiency is cell death around the time of fate conversion.

Different Modes of Cell Death and Oxidative Stress Limit Neuronal Reprogramming

While blocking apoptosis by caspase inhibitors and necroptosis by RIPK1 inhibitors significantly increased cell survival, these cell death pathways did not affect the proportion of iNs. This revealed an additional block for neuronal conversion that could be consistently relieved by ferroptosis inhibitors (Liproxstatin-1 or vitamin E). Ferroptosis is typically induced by ROS, resulting in peroxidation of lipids due to impaired cysteine availability, glutathione depletion and GPX4 inhibition (Dixon et al., 2012; Friedmann Angeli et al., 2014; Yang et al., 2014). Hence, excessive ROS may be generated as a consequence of instructing reprogramming per se or specifically into neurons that use oxidative phosphorylation. In favor of the former possibility are the findings of an oxidative burst with deleterious consequences during the generation of mouse iPSCs (Kida et al., 2015; Qi et al., 2015), initiated when cells are instructed to divide fast during reprogramming (Kida et al., 2015). This is notably different from direct neuronal reprogramming, where few cells divide and yet increased ROS and Lip-Ox occur. We therefore favor the hypothesis that this effect is due to transitioning too hastily to the neuronal oxidative metabolism during reprogramming (see also below).

Consistent with high oxidation levels limiting neuronal reprogramming efficiency, we show here that treatments beneficial for reprogramming, such as Fk or A(70)-Bcl-2, reduce Lip-Ox and mount an anti-oxidative response mediated by Nrf2 among others. Various agents attenuating Lip-Ox, such as αToc, αT3, or Calcitriol, also improve neuronal reprogramming. This is not only of crucial importance to better understand the conversion process into iNs but also for the widespread application of generating neurons from different cell types (astrocytes, MEFs, pericytes, etc.) with various neurogenic transcription factors (Ascl1, NeuroD4, Neurog2, Sox2, etc.) at much increased efficiency.

An Unexpected Role for Bcl-2 In Direct Neuronal Reprogramming

Interestingly, Bcl-2 affected both reprogramming efficiency and speed of neuronal conversion in a manner uncoupled from its function in apoptosis. The Bcl-2 mutant with increased affinity for Bax/Bak and therefore improved anti-apoptotic function (EE-*Bcl-2*) neither improved neuronal reprogramming nor reduced Lip-Ox. In contrast, A(145)- and A(70)-Bcl-2 mutants, unable to bind Bax/Bak and with reduced anti-apoptotic function (Deng et al., 2006; Yin et al., 1994), improved neuronal reprogramming, with the latter being the most effective in reducing Lip-Ox and, consequently, enhancing reprogramming efficiency. While this is the first time that specific Bcl-2 mutants have been used to assess selective effects on Lip-Ox, Bcl-2 has formerly been implicated in the regulation of both metabolic transition and oxidative stress pathways by reducing oxidation in mitochondria (Krishna et al., 2011) or improving metabolic conversion via interaction with, e.g., p53 or Myc (Deng et al., 2006; Jin et al., 2006). As EE-Bcl-2 interacts strongly with Bax, its lack of effect on reprogramming could be due to its reduced availability for molecular partners acting in the nucleus. Conversely, A(70)-Bcl-2 may be more efficient in improving neuronal reprogramming as more of this protein may be available in the nucleus for interaction with relevant partners.

Notably, we show that Fk and A(70)-Bcl-2 lead to common transcriptional changes in pathways (e.g., LXR) that have been previously implicated in neurogenesis (Theofilopoulos et al., 2013), suggesting that nuclear interactions of Bcl-2 may explain the particular efficiency of the A(70)-Bcl-2 mutant in direct neuronal reprogramming. Although not precluding additional roles of Bcl-2 at the mitochondria or other mechanisms, our data demonstrate that the effect of Bcl-2 in reprogramming is independent of its well-known anti-apoptotic function.

Metabolic Conversion as Critical Factor in Direct Neuronal Reprogramming

Importantly, factors alleviating Lip-Ox also accelerate fate transition. We observed this in vivo and by continuous single-cell tracking analysis in vitro, both upon Fk treatment and in cells co-expressing Bcl-2 (Figures 1 and S3). Fk treatment regulates several genes affecting the cellular redox potential, e.g., *Nor-1* that promotes the endurance phenotype in oxidative muscle fibers (Pearen et al., 2012) and *Vdr* that alleviates oxidative stress in various organs (Dong et al., 2012; George et al., 2012). It has been previously shown that ROS and redox-signaling mechanisms play a key role in cell fate decisions, including neurogenesis (Maryanovich and Gross, 2013; Prozorovski et al., 2015), although the molecular mechanisms mediating these effects are not yet fully understood. In iPSC reprogramming, changes to a more glycolytic metabolism have been shown to govern fate conversion (Liu et al., 2013b), despite the initial oxidative burst mentioned above (Kida et al., 2015). The faster neuronal conversion when excessive oxidation products are successfully controlled is consistent with (1) ROS affecting gene expression, e.g., by altering SIRT activity, a key regulator of neurogenesis, and (2) interfering with metabolic pathways acting upstream of other aspects of fate conversion. If the metabolic transition is a prerequisite for the conversion in cell fate, redox homeostasis failure may ultimately reduce efficiency or speed of conversion.

Confirming this hypothesis, we observed that cells cultured in a medium with oligomycin A, allowing anaerobic glycolysis as the only metabolic pathway to generate ATP (see Supplemental Information), preserved astroglial features and interfered with the conversion to a neuronal fate (Figures S7A–S7C, S7E, and S7F). As the total cell number did not decrease much (Figures S7A and S7F), fate conversion seems to be blocked when oxidative phosphorylation is hampered. Notably, cells grown in anaerobic glycolysis-only medium were also protected from Lip-Ox (Figures S7C and S7D), demonstrating that the metabolic change during neuronal reprogramming causes oxidative stress. Conversely, boosting the metabolic shift with a medium containing 2-deoxy-glucose, which can only be metabolized at mitochondria (see Supplemental Information), caused extraordinarily high levels of Lip-Ox (Figure S7C) in astrocytes and resulted in cell death (Figures S7A and S7F). Overall, these experiments demonstrate that the metabolic shift is not only necessary to allow survival of the neurons during reprogramming but also constitutes a prerequisite for cell fate transition.

Potent Improvement of Direct Reprogramming in the Injured Brain In Vivo

Importantly, αT3 supplementation or activation of anti-oxidant pathways by calcitriol was remarkably powerful in improving iN

maturation from reactive glia after traumatic brain injury in vivo. Interestingly, calcitriol treatment has been shown to reduce glutamate-induced neuronal death in vitro and attenuate hypoxic brain damage in vivo (Gianforcaro and Hamadeh, 2014), as well as the fibrotic reaction upon injury in other organs (Ding et al., 2013; Sherman et al., 2014). These data thus suggest that calcitriol alleviates several negative effects after injury. While both calcitriol and αT3 also improve efficiency of reprogramming but predominantly affect maturation and neurite growth, *Bcl-2* co-expression was the most efficient in increasing iNs. The combined action of Bcl-2 and Calcitriol or αT3 allowed us for the first time to achieve an in vivo reprogramming efficiency of more than 90% after stab wound injury. The neurons survived for several months and acquired a remarkably advanced state of maturation. These data demonstrate that the number of neurogenic fate determinants was not the limiting factor in neuronal reprogramming after injury in vivo, as believed so far. In fact, while applying various combinations of neurogenic transcription factors only marginally improved reprogramming in the same paradigm (Buffo et al., 2005; Grande et al., 2013; Heinrich et al., 2014; Kronenberg et al., 2010), co-expressing *Bcl-2* and alleviating excessive ROS had an astounding effect. Indeed, our protocol allowed iNs to proceed largely to a specific neuronal subtype, namely Ctip2+ pyramidal neurons even when they were located at more superficial positions and surrounded by Cux1+ upper layer neurons. Interestingly, *Ctip2* is not a direct target of Neurog2 (Masserdotti et al., 2015; Schuurmans et al., 2004) and acts as the key effector of subcortical deep layer neuron fate (Amamoto and Arlotta, 2014). Moreover, *Neurog2* knockout mice have selective defects in deep layer, but not upper-layer neurons of the developing cerebral cortex (Fode et al., 2000), supporting the concept that Neurog2 is largely involved in specifying deep-layer neuron fate in this region.

Taken together, our data on the mechanisms facilitating the metabolic transition and redox homeostasis in neuronal reprogramming have not only widespread relevance for brain injury and repair, but also highlight the urgency of improving the timely and coordinated metabolic conversion as well as protection from ferroptosis in aiming at neuronal repair.

EXPERIMENTAL PROCEDURES

Primary Cell Cultures

Astrocytes were cultured and transduced as described in Heinrich et al. (2010) and MEFs as described in Vierbuchen et al. (2010).

Live-Imaging Microscopy

Time-lapse video microscopy was performed with a cell observer (Zeiss) at a constant temperature of 37°C and 8% CO_2. Phase-contrast images were acquired every 5 min and fluorescence pictures every 4–6 hr for 6.5–7.5 days using a 10× phase contrast objective (Zeiss) and an AxioCam HRm camera with a self-written VBA module remote controlling Zeiss AxioVision 4.7 software. Movies were assembled and analyzed using ImageJ (NIH) software. For description of the analysis, see Supplemental Information.

Analysis of Lipid Peroxidation

For the detection of lipid peroxidation, we used either the reagent Click-iT lipid peroxidation kit based on linoleamide alkyne (LAA) reagent (Life Technologies) or BODIPY 581/591 C11 (C11-Bodipy, Molecular Probes; Drummen et al., 2002). Astroglial cells were first cultured and transfected as previously described (Heinrich et al., 2010; see also Supplemental Information). At 3.5 days later, the cells were labeled according to the specifications described in the product data sheet and fixed with 4% paraformaldehyde (PFA) for 5 min. Finally, the direct fluorescence of the reporters was detected by epi-florescent microscopy.

Animal Surgery

Operations were performed in accordance with the policies of the state of Bavaria under license number 55.2-1-54-2532-171-2011. Three days after performing a stab-wound injury, 0.5–1.0 μl of retroviral suspension (*Neurog2*-IRES-*RFP* alone or 1:1 with *Bcl-2*-IRES-*GFP*) was injected into the site of the lesion as described by Heinrich et al. (2014). When indicated in the text, 200 μl of Calcitriol (1 ng/μl, Tocris) or αT3 (100 mg/kg body weight; Sigma Aldrich) diluted in corn oil was administered through oral gavage at 2 DPI. The dosage was determined according with previous publications.

ACCESSION NUMBERS

Array data have been submitted to GEO under the accession number GEO: GSE70921.

SUPPLEMENTAL INFORMATION

Supplemental Information includes Supplemental Experimental Procedures, seven figures, four tables, and three movies and can be found with this article online at http://dx.doi.org/10.1016/j.stem.2015.12.003.

AUTHOR CONTRIBUTIONS

S.G. and M.G. conceived and designed the experiments; S.G., E.M., and M.G. designed in vivo experiments; E.M. performed in vivo experiments; S.G., F.O., A.D., G.L.R., and M.K. performed in vitro experiments; D.P. performed electrophysiological recordings; M.I., S.G., M.G., and G.M. performed genome-wide experiments and analysis; S.G., E.M., G.M., F.O., A.D., and G.L.R. analyzed data; G.M., M.I., J.B., J.P.F.A., M.C., C.B., T.S., and S.R. contributed reagents/materials/analysis tools; and M.G., S.G., E.M., and B.B. wrote the paper. All authors discussed the manuscript.

ACKNOWLEDGMENTS

We thank Tatjana Ebert, Carmen Meyer, Detlef Franzen, and Anke Pettenbrock for excellent technical assistance and Alex Lepier for advice with viral vector design. We are very grateful to Stefan Stricker, Leda Dimou, and Sofia Grade for excellent comments on the manuscript. Anti-Prx-AK was a kind gift of C.H. Lillig (Ernst-Moritz-Arndt-University, Greifswald, Germany). This work was supported by the German Research Foundation (M.G., GO 640/8-1, 10-1), the Helmholtz Portfolio Theme "Metabolic Dysfunction and Common Disease" (J.B.) and the Helmholtz Alliance "ICEMED" (J.B. and M.G.), the SFB 870 and the advanced ERC grant ChroNeuroRepair (M.G.), the grant "NewNeurons" (B.B. and M.G.) financed by the Ministry of Science and Education, and German Research Foundation Priority Program "Pluripotency and Reprogramming" (BE 4182/2-2 and GO 640/9-2).

Received: July 30, 2015
Revised: November 7, 2015
Accepted: December 10, 2015
Published: December 31, 2015

REFERENCES

Abdul-Muneer, P.M., Chandra, N., and Haorah, J. (2015). Interactions of oxidative stress and neurovascular inflammation in the pathogenesis of traumatic brain injury. Mol. Neurobiol. *51*, 966–979.

Amamoto, R., and Arlotta, P. (2014). Development-inspired reprogramming of the mammalian central nervous system. Science *343*, 1239882.

Anderová, M., Antonova, T., Petrík, D., Neprasová, H., Chvátal, A., and Syková, E. (2004). Voltage-dependent potassium currents in hypertrophied rat astrocytes after a cortical stab wound. Glia *48*, 311–326.

Arlotta, P., Molyneaux, B.J., Chen, J., Inoue, J., Kominami, R., and Macklis, J.D. (2005). Neuronal subtype-specific genes that control corticospinal motor neuron development in vivo. Neuron *45*, 207–221.

Bao, B.Y., Ting, H.J., Hsu, J.W., and Lee, Y.F. (2008). Protective role of 1 alpha, 25-dihydroxyvitamin D3 against oxidative stress in nonmalignant human prostate epithelial cells. Int. J. Cancer *122*, 2699–2706.

Berninger, B., Costa, M.R., Koch, U., Schroeder, T., Sutor, B., Grothe, B., and Götz, M. (2007). Functional properties of neurons derived from in vitro reprogrammed postnatal astroglia. J. Neurosci. *27*, 8654–8664.

Blum, R., Heinrich, C., Sánchez, R., Lepier, A., Gundelfinger, E.D., Berninger, B., and Götz, M. (2011). Neuronal network formation from reprogrammed early postnatal rat cortical glial cells. Cereb. Cortex *21*, 413–424.

Britanova, O., de Juan Romero, C., Cheung, A., Kwan, K.Y., Schwark, M., Gyorgy, A., Vogel, T., Akopov, S., Mitkovski, M., Agoston, D., et al. (2008). Satb2 is a postmitotic determinant for upper-layer neuron specification in the neocortex. Neuron *57*, 378–392.

Buettner, G.R. (1993). The pecking order of free radicals and antioxidants: lipid peroxidation, alpha-tocopherol, and ascorbate. Arch. Biochem. Biophys. *300*, 535–543.

Buffo, A., Vosko, M.R., Ertürk, D., Hamann, G.F., Jucker, M., Rowitch, D., and Götz, M. (2005). Expression pattern of the transcription factor Olig2 in response to brain injuries: implications for neuronal repair. Proc. Natl. Acad. Sci. USA *102*, 18183–18188.

Chanda, S., Ang, C.E., Davila, J., Pak, C., Mall, M., Lee, Q.Y., Ahlenius, H., Jung, S.W., Südhof, T.C., and Wernig, M. (2014). Generation of induced neuronal cells by the single reprogramming factor ASCL1. Stem Cell Reports *3*, 282–296.

Degterev, A., Huang, Z., Boyce, M., Li, Y., Jagtap, P., Mizushima, N., Cuny, G.D., Mitchison, T.J., Moskowitz, M.A., and Yuan, J. (2005). Chemical inhibitor of nonapoptotic cell death with therapeutic potential for ischemic brain injury. Nat. Chem. Biol. *1*, 112–119.

Deng, X., Gao, F., Flagg, T., Anderson, J., and May, W.S. (2006). Bcl2's flexible loop domain regulates p53 binding and survival. Mol. Cell. Biol. *26*, 4421–4434.

Ding, N., Yu, R.T., Subramaniam, N., Sherman, M.H., Wilson, C., Rao, R., Leblanc, M., Coulter, S., He, M., Scott, C., et al. (2013). A vitamin D receptor/SMAD genomic circuit gates hepatic fibrotic response. Cell *153*, 601–613.

Dixon, S.J., Lemberg, K.M., Lamprecht, M.R., Skouta, R., Zaitsev, E.M., Gleason, C.E., Patel, D.N., Bauer, A.J., Cantley, A.M., Yang, W.S., et al. (2012). Ferroptosis: an iron-dependent form of nonapoptotic cell death. Cell *149*, 1060–1072.

Dong, J., Wong, S.L., Lau, C.W., Lee, H.K., Ng, C.F., Zhang, L., Yao, X., Chen, Z.Y., Vanhoutte, P.M., and Huang, Y. (2012). Calcitriol protects renovascular function in hypertension by down-regulating angiotensin II type 1 receptors and reducing oxidative stress. Eur. Heart J. *33*, 2980–2990.

Drummen, G.P., van Liebergen, L.C., Op den Kamp, J.A., and Post, J.A. (2002). C11-BODIPY(581/591), an oxidation-sensitive fluorescent lipid peroxidation probe: (micro)spectroscopic characterization and validation of methodology. Free Radic. Biol. Med. *33*, 473–490.

Fode, C., Ma, Q., Casarosa, S., Ang, S.L., Anderson, D.J., and Guillemot, F. (2000). A role for neural determination genes in specifying the dorsoventral identity of telencephalic neurons. Genes Dev. *14*, 67–80.

Friedmann Angeli, J.P., Schneider, M., Proneth, B., Tyurina, Y.Y., Tyurin, V.A., Hammond, V.J., Herbach, N., Aichler, M., Walch, A., Eggenhofer, E., et al. (2014). Inactivation of the ferroptosis regulator Gpx4 triggers acute renal failure in mice. Nat. Cell Biol. *16*, 1180–1191.

George, N., Kumar, T.P., Antony, S., Jayanarayanan, S., and Paulose, C.S. (2012). Effect of vitamin D3 in reducing metabolic and oxidative stress in the liver of streptozotocin-induced diabetic rats. Br. J. Nutr. *108*, 1410–1418.

Gianforcaro, A., and Hamadeh, M.J. (2014). Vitamin D as a potential therapy in amyotrophic lateral sclerosis. CNS Neurosci. Ther. *20*, 101–111.

Godoy, J.R., Oesteritz, S., Hanschmann, E.M., Ockenga, W., Ackermann, W., and Lillig, C.H. (2011). Segment-specific overexpression of redoxins after renal ischemia and reperfusion: protective roles of glutaredoxin 2, peroxiredoxin 3, and peroxiredoxin 6. Free Radic. Biol. Med. *51*, 552–561.

Grande, A., Sumiyoshi, K., López-Juárez, A., Howard, J., Sakthivel, B., Aronow, B., Campbell, K., and Nakafuku, M. (2013). Environmental impact on direct neuronal reprogramming in vivo in the adult brain. Nat. Commun. *4*, 2373.

Guo, Z., Zhang, L., Wu, Z., Chen, Y., Wang, F., and Chen, G. (2014). In vivo direct reprogramming of reactive glial cells into functional neurons after brain injury and in an Alzheimer's disease model. Cell Stem Cell *14*, 188–202.

Halley-Stott, R.P., Jullien, J., Pasque, V., and Gurdon, J. (2014). Mitosis gives a brief window of opportunity for a change in gene transcription. PLoS Biol. *12*, e1001914.

Heinrich, C., Blum, R., Gascón, S., Masserdotti, G., Tripathi, P., Sánchez, R., Tiedt, S., Schroeder, T., Götz, M., and Berninger, B. (2010). Directing astroglia from the cerebral cortex into subtype specific functional neurons. PLoS Biol. *8*, e1000373.

Heinrich, C., Bergami, M., Gascón, S., Lepier, A., Viganò, F., Dimou, L., Sutor, B., Berninger, B., and Götz, M. (2014). Sox2-mediated conversion of NG2 glia into induced neurons in the injured adult cerebral cortex. Stem Cell Reports *3*, 1000–1014.

Imayoshi, I., and Kageyama, R. (2014). bHLH factors in self-renewal, multipotency, and fate choice of neural progenitor cells. Neuron *82*, 9–23.

Jin, Z., May, W.S., Gao, F., Flagg, T., and Deng, X. (2006). Bcl2 suppresses DNA repair by enhancing c-Myc transcriptional activity. J. Biol. Chem. *281*, 14446–14456.

Kawamura, T., Suzuki, J., Wang, Y.V., Menendez, S., Morera, L.B., Raya, A., Wahl, G.M., and Izpisúa Belmonte, J.C. (2009). Linking the p53 tumour suppressor pathway to somatic cell reprogramming. Nature *460*, 1140–1144.

Kida, Y.S., Kawamura, T., Wei, Z., Sogo, T., Jacinto, S., Shigeno, A., Kushige, H., Yoshihara, E., Liddle, C., Ecker, J.R., et al. (2015). ERRs Mediate a Metabolic Switch Required for Somatic Cell Reprogramming to Pluripotency. Cell Stem Cell *16*, 547–555.

Krishna, S., Low, I.C., and Pervaiz, S. (2011). Regulation of mitochondrial metabolism: yet another facet in the biology of the oncoprotein Bcl-2. Biochem. J. *435*, 545–551.

Kronenberg, G., Gertz, K., Cheung, G., Buffo, A., Kettenmann, H., Götz, M., and Endres, M. (2010). Modulation of fate determinants Olig2 and Pax6 in resident glia evokes spiking neuroblasts in a model of mild brain ischemia. Stroke *41*, 2944–2949.

Liu, M.L., Zang, T., Zou, Y., Chang, J.C., Gibson, J.R., Huber, K.M., and Zhang, C.L. (2013a). Small molecules enable neurogenin 2 to efficiently convert human fibroblasts into cholinergic neurons. Nat. Commun. *4*, 2183.

Liu, W., Long, Q., Chen, K., Li, S., Xiang, G., Chen, S., Liu, X., Li, Y., Yang, L., Dong, D., et al. (2013b). Mitochondrial metabolism transition cooperates with nuclear reprogramming during induced pluripotent stem cell generation. Biochem. Biophys. Res. Commun. *431*, 767–771.

Maryanovich, M., and Gross, A. (2013). A ROS rheostat for cell fate regulation. Trends Cell Biol. *23*, 129–134.

Masserdotti, G., Gillotin, S., Sutor, B., Drechsel, D., Irmler, M., Jørgensen, H.F., Sass, S., Theis, F.J., Beckers, J., Berninger, B., et al. (2015). Transcriptional Mechanisms of Proneural Factors and REST in Regulating Neuronal Reprogramming of Astrocytes. Cell Stem Cell *17*, 74–88.

McKay, N.D., Robinson, B., Brodie, R., and Rooke-Allen, N. (1983). Glucose transport and metabolism in cultured human skin fibroblasts. Biochim. Biophys. Acta *762*, 198–204.

Molyneaux, B.J., Arlotta, P., Menezes, J.R., and Macklis, J.D. (2007). Neuronal subtype specification in the cerebral cortex. Nat. Rev. Neurosci. *8*, 427–437.

Nguyen, T., Nioi, P., and Pickett, C.B. (2009). The Nrf2-antioxidant response element signaling pathway and its activation by oxidative stress. J. Biol. Chem. *284*, 13291–13295.

Ninkovic, J., Steiner-Mezzadri, A., Jawerka, M., Akinci, U., Masserdotti, G., Petricca, S., Fischer, J., von Holst, A., Beckers, J., Lie, C.D., et al. (2013). The BAF complex interacts with Pax6 in adult neural progenitors to establish

a neurogenic cross-regulatory transcriptional network. Cell Stem Cell *13*, 403–418.

Niu, W., Zang, T., Zou, Y., Fang, S., Smith, D.K., Bachoo, R., and Zhang, C.L. (2013). In vivo reprogramming of astrocytes to neuroblasts in the adult brain. Nat. Cell Biol. *15*, 1164–1175.

Park, S.K., Dahmer, M.K., and Quasney, M.W. (2012). MAPK and JAK-STAT signaling pathways are involved in the oxidative stress-induced decrease in expression of surfactant protein genes. Cell. Physiol. Biochem. *30*, 334–346.

Pearen, M.A., Eriksson, N.A., Fitzsimmons, R.L., Goode, J.M., Martel, N., Andrikopoulos, S., and Muscat, G.E. (2012). The nuclear receptor, Nor-1, markedly increases type II oxidative muscle fibers and resistance to fatigue. Mol. Endocrinol. *26*, 372–384.

Pedroni, A., Minh, D., Mallamaci, A., and Cherubini, E. (2014). Electrophysiological characterization of granule cells in the dentate gyrus immediately after birth. Front. Cell. Neurosci. *8*, 44.

Prozorovski, T., Schneider, R., Berndt, C., Hartung, H.P., and Aktas, O. (2015). Redox-regulated fate of neural stem progenitor cells. Biochim. Biophys. Acta *1850*, 1543–1554.

Qi, S., Fang, Z., Wang, D., Menendez, P., Yao, K., and Ji, J. (2015). Concise review: induced pluripotency by defined factors: prey of oxidative stress. Stem Cells *33*, 1371–1376.

Ruiz, S., Panopoulos, A.D., Herrerías, A., Bissig, K.D., Lutz, M., Berggren, W.T., Verma, I.M., and Izpisua Belmonte, J.C. (2011). A high proliferation rate is required for cell reprogramming and maintenance of human embryonic stem cell identity. Curr. Biol. *21*, 45–52.

Schuurmans, C., Armant, O., Nieto, M., Stenman, J.M., Britz, O., Klenin, N., Brown, C., Langevin, L.M., Seibt, J., Tang, H., et al. (2004). Sequential phases of cortical specification involve Neurogenin-dependent and -independent pathways. EMBO J. *23*, 2892–2902.

Sherman, M.H., Yu, R.T., Engle, D.D., Ding, N., Atkins, A.R., Tiriac, H., Collisson, E.A., Connor, F., Van Dyke, T., Kozlov, S., et al. (2014). Vitamin D receptor-mediated stromal reprogramming suppresses pancreatitis and enhances pancreatic cancer therapy. Cell *159*, 80–93.

Theofilopoulos, S., Wang, Y., Kitambi, S.S., Sacchetti, P., Sousa, K.M., Bodin, K., Kirk, J., Saltó, C., Gustafsson, M., Toledo, E.M., et al. (2013). Brain endogenous liver X receptor ligands selectively promote midbrain neurogenesis. Nat. Chem. Biol. *9*, 126–133.

Torper, O., Pfisterer, U., Wolf, D.A., Pereira, M., Lau, S., Jakobsson, J., Björklund, A., Grealish, S., and Parmar, M. (2013). Generation of induced neurons via direct conversion in vivo. Proc. Natl. Acad. Sci. USA *110*, 7038–7043.

Tsacopoulos, M., and Magistretti, P.J. (1996). Metabolic coupling between glia and neurons. J. Neurosci. *16*, 877–885.

Vierbuchen, T., Ostermeier, A., Pang, Z.P., Kokubu, Y., Sudhof, T.C., and Wernig, M. (2010). Direct conversion of fibroblasts to functional neurons by defined factors. Nature *463*, 1035–1041.

Wapinski, O.L., Vierbuchen, T., Qu, K., Lee, Q.Y., Chanda, S., Fuentes, D.R., Giresi, P.G., Ng, Y.H., Marro, S., Neff, N.F., et al. (2013). Hierarchical mechanisms for direct reprogramming of fibroblasts to neurons. Cell *155*, 621–635.

Yang, W.S., SriRamaratnam, R., Welsch, M.E., Shimada, K., Skouta, R., Viswanathan, V.S., Cheah, J.H., Clemons, P.A., Shamji, A.F., Clish, C.B., et al. (2014). Regulation of ferroptotic cancer cell death by GPX4. Cell *156*, 317–331.

Yin, X.M., Oltvai, Z.N., and Korsmeyer, S.J. (1994). BH1 and BH2 domains of Bcl-2 are required for inhibition of apoptosis and heterodimerization with Bax. Nature *369*, 321–323.

Zhang, J., Nuebel, E., Daley, G.Q., Koehler, C.M., and Teitell, M.A. (2012). Metabolic regulation in pluripotent stem cells during reprogramming and self-renewal. Cell Stem Cell *11*, 589–595.